



HAL
open science

Study of consecutive long-lived meter-scale laser-guided sparks in air

Pierre Walch, Leonid Arantchouk, Benoit Mahieu, Magali Lozano,
Yves-Bernard André, André Mysyrowicz, Aurélien Houard

► **To cite this version:**

Pierre Walch, Leonid Arantchouk, Benoit Mahieu, Magali Lozano, Yves-Bernard André, et al.. Study of consecutive long-lived meter-scale laser-guided sparks in air. *Physics of Plasmas*, 2023, 30 (8), pp.083503. 10.1063/5.0146392 . hal-04176299

HAL Id: hal-04176299

<https://hal.science/hal-04176299>

Submitted on 2 Aug 2023

HAL is a multi-disciplinary open access archive for the deposit and dissemination of scientific research documents, whether they are published or not. The documents may come from teaching and research institutions in France or abroad, or from public or private research centers.

L'archive ouverte pluridisciplinaire **HAL**, est destinée au dépôt et à la diffusion de documents scientifiques de niveau recherche, publiés ou non, émanant des établissements d'enseignement et de recherche français ou étrangers, des laboratoires publics ou privés.

Study of consecutive long-lived meter-scale laser guided sparks in air

P. Walch,¹ L. Arantchouk,¹ B. Mahieu,¹ M. Lozano,¹ Y.-B. André,¹ A. Mysyrowicz,¹ and A. Houard¹
 LOA, ENSTA Paris, CNRS, École Polytechnique, Institut Polytechnique de Paris, 828 Bd des Maréchaux, 91762 Palaiseau, France

(*Electronic mail: pierre.walch@ensta-paris.fr)

(Dated: 15 June 2023)

We study the creation and evolution of meter-scale long-lived laser guided electric discharges and the interaction between consecutive guided discharges. The lifetime of guided discharges from a Tesla HV generator is first increased up to several milliseconds by injection of additional current. The subsequent discharge evolution is measured by recording the electric current and by Schlieren and fluorescence imaging. A thermodynamic model of the gas evolution is developed to explain the discharge evolution. Finally, we analyze the succession of laser guided discharges generated at 10 Hz.

During the last decades, femtosecond laser filamentation¹ has been used to reliably trigger and guide electric discharges in the atmosphere^{2–6}. Through reduction of the gas density and generation of long-lived charges, the plasma channel created by the filament forms a preferential path for any streamer or leader propagating in air^{3,7–10}. Several applications have been proposed for this spectacular effect, such as the laser lightning rod⁶, the laser triggered Marx generator¹¹ or the plasma antenna^{12,13}. The main limitation for the later application is the short discharge lifetime, since a plasma antenna would require the existence of a permanent conductive channel. Discharges generated by high voltage generators cannot deliver currents exceeding a few microseconds¹⁴. These generators are typically Marx generators³ or Tesla generators^{13,15}. To increase the lifetime of the conductive channel, a technique consists in combining a high voltage generator together with an energetic current generator to maintain the laser guided discharge. Demonstrated by Arantchouk et al.¹⁴, this method has been improved to the millisecond duration by Theberge et al.¹⁶. For longer plasma lifetime, two approaches are possible: either increase the capacitance of the secondary current generator or realize successive laser guided discharges.

In this paper, we characterize the evolution of a long-lived discharge triggered by laser filamentation and generated by a Tesla coil and a secondary current circuit. Several measurement methods are used and a model is developed to explain the evolution of the discharge that lasts for several ms. Then, we study the guiding of two subsequent discharges separated by 100 ms. The study of such a regime combining a long discharge lifetime and a high repetition rate could create a quasi-permanent conductive discharge in air, an ideal tool for a plasma antenna^{12,13}.

A. Experimental setup

To create the filaments a laser pulse with an energy of 200 mJ, a pulse duration of 780 fs, at a central wavelength of 800 nm is focused in air through a 7 m converging lens. A bundle of filaments of 1.5 m length is formed before the geometrical focus of the lens, connecting two electrodes separated by 80 cm as presented in Fig. 1(a). A 300 kV high voltage Tesla generator synchronized with the laser (see description in¹⁵)

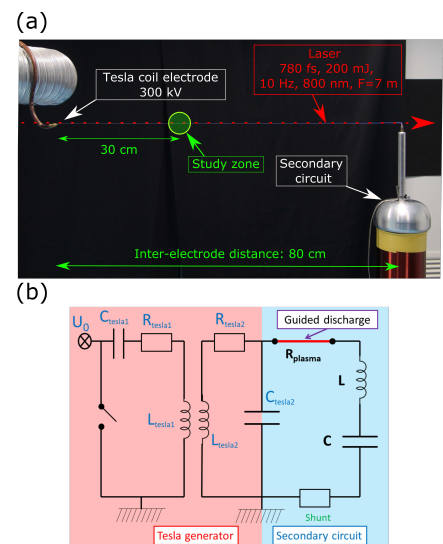


FIG. 1. (a) Experimental setup. A 200 mJ, 780 fs, 800 nm laser pulse is focused in air with a 7 m lens and produces filaments between two electrodes separated by 80 cm. A 300-kV high voltage pulse generated by a Tesla coil and synchronized with the laser creates a discharge between the two electrodes. A secondary electric circuit injects additional current into the discharge to increase the discharge lifetime. The resulting long-lived discharges are characterized by current measurements and with fluorescence and Schlieren imaging of a study zone 30 cm away from the Tesla electrode. (b) Electrical diagram of the setup. The tesla generator (represented in red) is fully described in [12]. The secondary circuit (represented in blue) is composed of a coil $L = 47.8$ mH, a capacitance C varying from 350 to 720 nF charged at 20 kV and by the discharge with resistance R_{plasma} . A shunt is present in the circuit to allow the measurement of the discharge current.

delivers a voltage pulse on the left electrode while the second one is connected to an oscillating circuit (designed as “secondary circuit”) used to inject additional current into the dis-

charge to increase its lifetime, as presented in Fig. 1(b). This secondary circuit is composed of a coil $L = 47.8$ mH, a capacitance C varying from 350 to 720 nF charged at 20 kV and by the discharge with resistance R_{plasma} . By varying the value of this capacitance, the amount of current injected is varied and the plasma lifetime is then increased. When a laser filament is produced between the two electrodes during a maximum of the Tesla voltage a guided discharge is produced between the two electrodes with a reduced breakdown voltage¹⁷, as presented in Fig. 2(a).

This guided discharge is characterized by several diagnostics. A shunt is present in the electrical system to record the electrical current passing through the discharge. A Schlieren imaging setup records the temporal evolution of the discharge radius by using a probe laser pulse at 640 nm with a duration of 1 s collimated to study a zone of 3 cm diameter. This laser is sent perpendicularly through the discharge at a distance $D = 33$ cm from the Tesla electrode to avoid any point effect due to the electrode. A high-speed camera, model Fastcam SA-X2 from Photron, set at a frequency of 40 000 images/s is used to record the Schlieren images. The probe laser is synchronized with the high-speed camera. A narrow band filter, centered at 640 nm, is placed in front of the camera to reduce the perturbation due to the light emitted by the discharge. A characterization of the air density variation induced by the guided discharge and by the filamentation is realized by using the previously described probe laser setup and by sending it toward a Phasics SID4 wavefront sensor. This measurement is repeated at different positions along the filamentation zone to fully evaluate the filamentation under dense channel responsible for the guiding of the discharge. Spectroscopic measurement of the light emitted by the discharge is realized at different time delays during the discharge lifetime using a spectrometer Acton SP2756 from Princeton Instruments.

B. Characterization of the long-lived laser guided discharge

Measurements of the current in the discharge for three values of capacitance 350 nF, 540 nF and 720 nF are presented in Fig. 2 (b). They show an increase of the current peak value and duration as the capacitance is increased. These signals were fitted with the damped wave function of an RLC circuit. The value of L and C are given by the parameters of the electrical setup (see Fig. 1(b)), and the value of R of the discharge resistance is adjusted for a best fit and considered constant during the discharge. A constant resistance gives a good match with the experimental observations during the entire discharge, as observed previously¹⁸. This analysis yields the values of the discharge resistance, respectively 240 Ohm for a capacitance of 350 nF, 175 Ohm for 540 nF and 147 Ohm for 720 nF. The decrease of the resistance as the capacitance increases can be explained by an increase of the conductivity of the plasma when the current is increased.

To analyze the plasma column, we simulate the evolution of the discharge temperature T based on the evolution of the

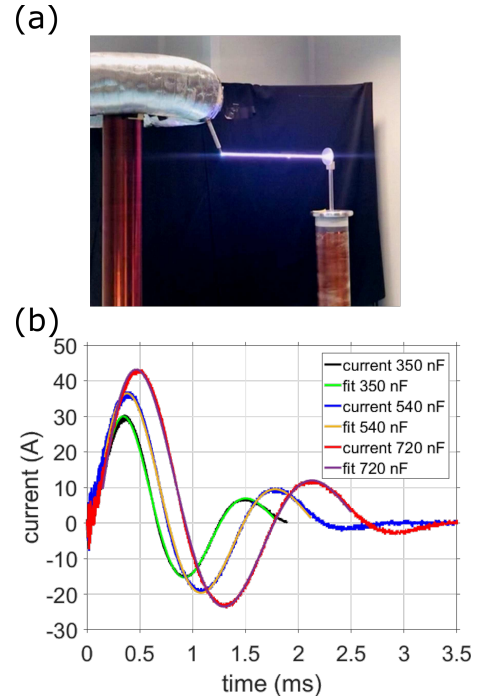


FIG. 2. (a) Picture of the laser guided discharge. (b) Current flowing in the discharge measured for the three values of capacitance, and corresponding fits.

enthalpy H of the discharge system:

$$\frac{dH}{dt} = \frac{dU}{dt} + P \frac{dV}{dt}, \quad (1)$$

with U the internal energy of the system, P the pressure of the system being equal to the ambient pressure, and V the volume of the discharge. Note that there is no term related to the evolution of the pressure because the system is at pressure equilibrium with the ambient pressure during the considered time scale.

The temporal evolution of the internal energy of the system is described by identifying the terms involved in the energy balance of the Elenbaas-Heller equation, resulting in the equation:

$$\begin{aligned} \frac{dU}{dt} = & \iiint_V \frac{1}{r} \frac{\partial}{\partial r} (r \times \lambda(T) \times \frac{\partial T(r,t)}{\partial r}) dV \\ & + \iiint_V \sigma(T) \times E(t)^2 dV \\ & - \iiint_V Q_r(r,T) dV, \end{aligned} \quad (2)$$

With r the discharge radius, λ the thermal conductivity of air, σ the electrical conductivity, E the electrical field strength and Q_r the volumetric power of radiation losses.

Each three term is then simplified using the following hypotheses:

- The first term related to the air thermal conductivity, that will be named $P_{thermalconductivity}(t)$, is transformed using the Green-Ostrogradsky's theorem. Furthermore, the discharge is assumed to be a cylinder with a Gaussian radial profile of temperature, and we consider it invariant along its length by neglecting the point effect of the electrodes:

$$\begin{aligned} & \iiint_V \frac{1}{r} \frac{\partial}{\partial r} (r \times \lambda(T) \times \frac{\partial T(r,t)}{\partial r}) dV \\ &= \iint_S \lambda(T_{FWHM}(t)) \times \frac{\partial T(r,t)}{\partial r} |_{FWHM(t)} dS \\ &= \lambda(T_{FWHM}(t)) \times \frac{\partial T(r,t)}{\partial r} |_{FWHM(t)} \times S \\ &= P_{thermalconductivity}(t), \end{aligned} \quad (3)$$

- The second term related to the energy gain by joule effect, that will be named $P_{electricgain}(t)$, is evaluated using the previously described measured value of the discharge resistance R_{ohm} , and of the measured current i :

$$\begin{aligned} \iiint_V \sigma(T) \times E(t)^2 dV &= R_{ohm} \times i(t)^2 \\ &= P_{electricgain}(t), \end{aligned} \quad (4)$$

- The third term represents the radiation losses of grey body, that will be named $P_{radiative}(t)$, can be written as:

$$\begin{aligned} \iiint_V Q_r(r,T) dV &= S(t) \times \epsilon \times \sigma_b \times T_{FWHM}^4 \\ &= P_{radiative}(t), \end{aligned} \quad (5)$$

with S the surface of the discharge, ϵ the grey body emissivity, σ_b the Stefan-Boltzmann constant and T_{FWHM} the discharge temperature at the FWHM position.

We then use these terms and integrate the equation (1) using a first order Euler method. All the radiation constants and transport properties are interpolated from the values of the tables from^{19,20} and used as input in the code to be evaluated at each time step.

The evolution of the system is then described by the two equations:

$$\begin{aligned} & \Delta T(t) \times c_p \times \pi \times L \times R(t)^2 \times \rho(t) \\ & - \Delta T(t_0) \times c_p \times \pi \times L \times R(t_0)^2 \times \rho(t_0) \\ & = P \times \pi \times L \times (R(t)^2 - R(t_0)^2) \\ & + \int_{t_0}^t (P_{electricgain} - (P_{thermalconductivity} + P_{radiative})) dt, \end{aligned} \quad (6)$$

$$R(t+dt) = R(t) + \frac{4 \times \alpha(\Delta T(t))}{2 \times R(t)}. \quad (7)$$

with ΔT the temperature variation at the FWHM position, c_p the air isobaric specific heat, L the length of the discharge (in our case, 80 cm), ρ the air density, R the discharge radius defined as the position of the FWHM of the Gaussian temperature profile, P the ambient pressure, α the air thermal diffusivity, and t_0 the starting time of the simulation.

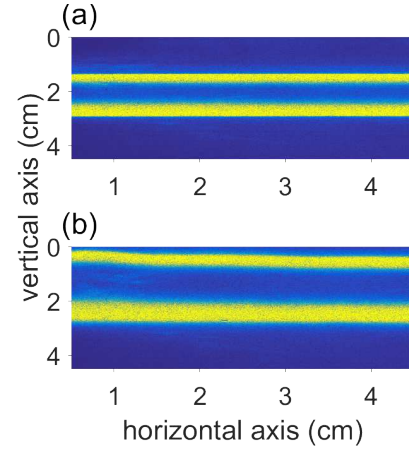


FIG. 3. Schlieren images of the guided discharge recorded (a) 5 ms and (b) 100 ms after the discharge initiation, for a capacitance value $C = 720$ nF. The edges of the discharge, represented in yellow, stay straight during the recorded period of 100 ms.

Using this model, we simulate the evolution of the discharge radius and of the discharge temperature over 2.5 ms for the three values of capacitance in the secondary circuit. The simulation starts 0.3 ms after the beginning of the discharge since our model does not take into account the initial evolution resulting from the Tesla discharge. Over this time period, the discharge has reached LTE (local thermodynamic equilibrium) and can be described as a single temperature fluid. Using Schlieren imaging, we capture images of the evolution at a rate of 40 000 frames/s and retrieve from these measurements the evolution of the discharge radius. The first important observation is that the post discharges channel stay straight during all its lifetime recorded up to 100 ms, as presented in Fig. 3. Moreover, the comparison between the simulated and measured evolution of the channel radius, presented in Fig. 4(a), shows a good match for all tested values of capacitance in the secondary circuit. We attribute the slight difference observed between measurement and calculation here to the limit of validity of the hypothesis of a constant resistance for the discharge.

The simulated evolution of the temperature at the discharge center is presented in Fig. 4(b). The results show a clear distinction between discharges with and without the secondary circuit: without the secondary circuit, the temperature returns to room temperature in less than a millisecond, while the use of the secondary circuit increases both the maximum of tem-

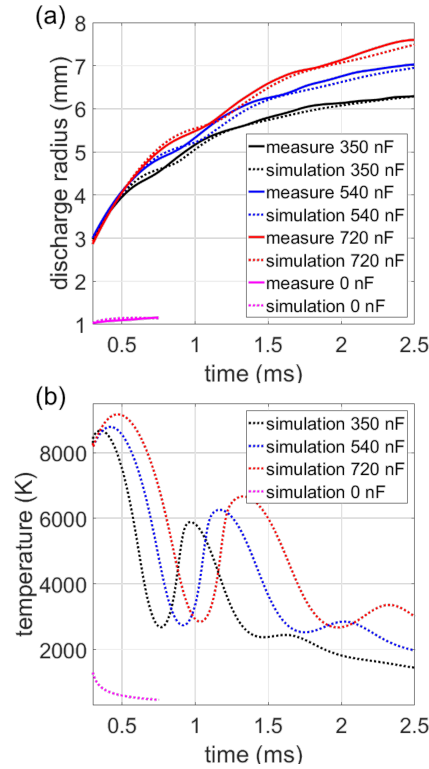


FIG. 4. (a) Measured (continuous line) and simulated (dotted line) temporal evolution of the discharges radius for different capacitance values C in the secondary circuit. (b) Simulated discharge temperatures for different capacitance values in the secondary circuit.

perature and the time during which the discharge temperature stays high.

To validate our model for temperature evolution, we performed a spectroscopic measurement of the light emitted by the discharge during the first and the second ms with a capacitance $C = 720$ nF. The results, presented in Fig. 5(a), were fitted using the Specair program²¹ to retrieve the discharge temperature. We analyzed the plasma evolution at the millisecond timescale, which is order of magnitude greater than the electron collision frequency at atmospheric pressure. Therefore, the discharge was considered as a single-temperature fluid and the electronic, rotational, translational and vibrational temperatures were considered at equilibrium. We obtain temperatures of 7 350 K and 5 500 K for the first and second milliseconds, respectively. These values are compared to the root mean fourth power $\sqrt[4]{\langle \Delta T^4 \rangle}$ and are consistent with the values given by the simulation of 7 830 K and 5 420 K, for the time period from 0.3 to 1 ms and 1 to 2 ms, respectively

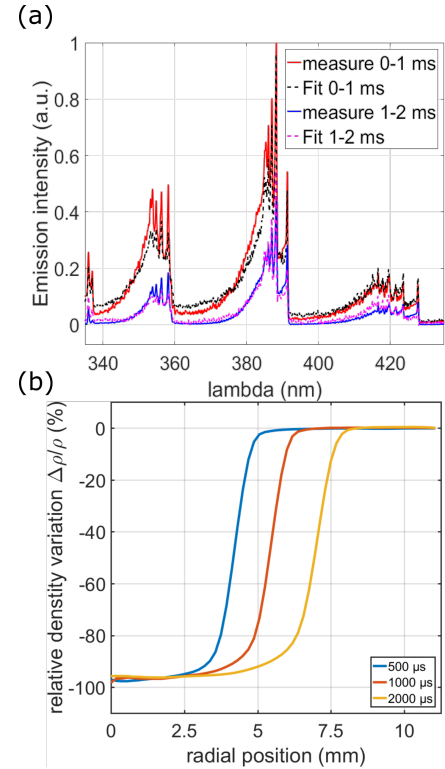


FIG. 5. (a) Measured and fitted emission spectrum of the discharge, for the first and second ms after the beginning of the discharge, for $C = 720$ nF. (b) Measured radial profiles of the air density variation in the discharge for $C = 720$ nF, measured at a delay of 500 μ s (in blue), 1000 μ s (in orange) and 2000 μ s (in blue) after the beginning of the discharge.

and are in the same range as similar discharges previously observed by Theberge et al.¹⁶.

In addition, the temperature radial profile of the discharge was evaluated using a transverse interferometry technique. By sending a probe beam perpendicularly through the discharge, we measured the index phase shift variation. Note that this measurement includes both the phase shift induced by the electrons present in the discharge and the air density variation, so the quantitative values of the density variation presented in Fig. 5(b) are not valid. However, it gives us insight about the radial profile of the density variation and by extension, of the temperature profile, the system being at the pressure equilibrium at the studied timescale¹⁶. The measurement was repeated for delays of 0.5, 1 and 2 ms after the beginning of the discharge. The result, presented in Fig. 5(b), gives the same value of radius as the ones resulting from the simulation and

the ones measured by Schlieren imaging, and show profiles that are consistent with the model hypothesis.

We now discuss the light emitted by the discharge. Our model of discharge evolution only takes into account the light emitted as a form of a grey body radiation, while our spectroscopic measurement shows the presence of spectral lines. While this is a contradiction, it does not change the validity of our model because the losses by radiation are negligible in the energy balance for the temperature range of our discharges. The radiation of the discharges was further measured by taking pictures of the emitted light with a high-speed camera (Fastcam SA-X2 from Photron) recording 50 000 frames per second. With this setup, a 20 cm portion of the discharge located in the middle of the electrode gap was examined (note however, that we checked that the plasma evolution was homogeneous along the discharge axis except close to the electrodes).

From these measurements, the temporal evolution of two main parameters was retrieved: the total flux of light emitted by the discharge, made by integrating the signal over the entire captured images, and the light width, calculated by taking the FWHM of the radial profile of the emitted light intensity and by averaging it over the 20 cm of the observed discharge. The measurements were repeated for the capacitance values in the secondary circuit $C = 350$ nF, 540 nF and 720 nF.

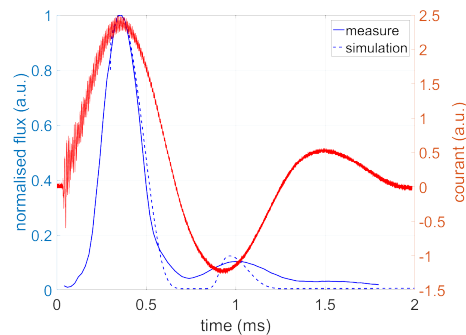


FIG. 6. Normalised measured luminous flux (blue continuous line) compared to the normalised simulated luminous flux (dashed blue line) for a discharge obtained with a capacitance value $C = 350$ nF. The corresponding measured current is also shown in red.

As shown in Fig. 6, the evolution of the flux emitted by the discharge presents maxima when the current is maximum, but the amplitude of these maxima decreases faster than the current. This flux temporal evolution is well reproduced by our model for the evolution of the discharge (dashed line in Fig. 6).

The observation of the width of the emitted light, as commonly used in previous research studies of laser guided discharges¹³, shows a surprising temporal evolution: rather than a continuous increase similar to the discharge radius measured by schlieren imaging (Fig. 4(a)), an initial slow increase is observed, followed by a rapid jump, followed by a second

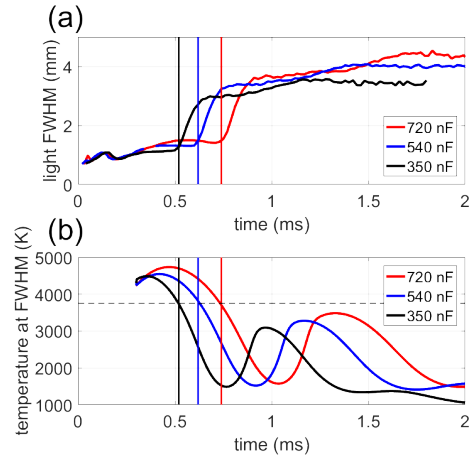


FIG. 7. (a) Measured temporal evolution of the light width (FWHM) emitted by the discharge for capacitance values in the secondary circuit $C = 720$ nF, 540 nF, and 350 nF. (b) Corresponding simulated temperature on the discharge width. On each subfigure, the vertical lines indicate the beginning of the jump in the measured emitted light width.

slow increase, as presented in Fig. 7(a). The light width shows an increase by a ratio of ≈ 2.5 during the jump and this ratio is the same for all capacitance values C . Its temporal position is delayed as C is increased, but it is not synchronized with the discharge current. We do not have a full explanation of this phenomenon as we do not have a full identification of the light emission processes involved. However, the jump seems to be correlated with the temperature of the discharge. Using our model, we simulate the discharge temperature at its FWHM and compare it to the temporal evolution of the emitted light width. The results, presented in Fig. 7(b), show that the jump precisely appears when the temperature drops below 3750 K. We therefore hypothesize the behavior of the discharge light emission as follows: We consider two emission processes, with the first being dependent on temperature to a higher order than the second one. During the initial stage of the discharge, the temperature is high and thus the higher order emission is predominant and dictates the light width evolution. The later part of the discharge is at lower temperature and the low order emission becomes predominant. The jump is thus characteristic of the transition from one predominant emission process to another one. We do not know the nature of these two emission processes, but we infer that the high order emission is related to air ionization, and might correspond to grey body radiation while the observed temperature threshold of 3750 K suggests that the other one is related predominantly to the emission from spectral lines (we note that $T = 3750$ K corresponds to the onset of ionization from NO^+).

C. Consecutive discharges

We now analyse the generation of consecutive millisecond laser-guided discharges separated by 100 ms using a laser system working at 10 Hz. We first generated consecutive discharges without using the secondary circuit ($C = 0$). This test was successful and 4 consecutive short discharges were confirmed to be guided. By using the Schlieren imaging setup previously described, we observed that all these 4 discharges were having similar evolution and no interaction between discharges was observed.

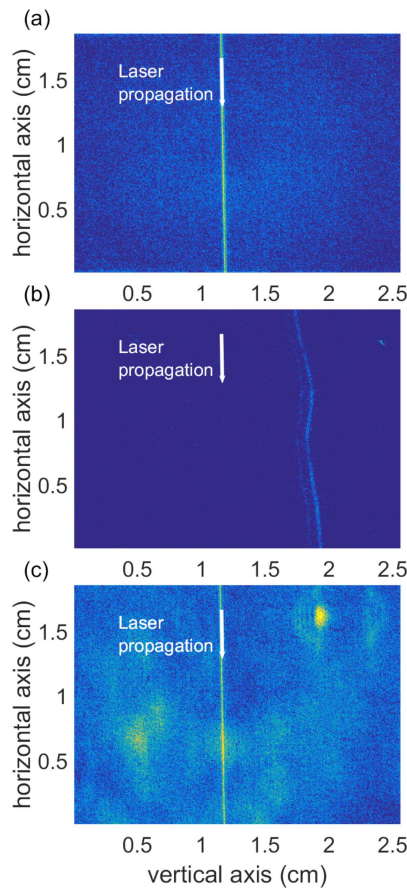


FIG. 8. Schlieren imaging of a long discharge followed by a second discharge 100 ms after. (a) image of the first discharge, (b) image of the second discharge. Note that in the second image, the background noise is subtracted to distinguish the discharge path. (c) Image of the second discharge in the presence of an airflow.

The second test consisted in generating consecutive dis-

charges using the secondary circuit to increase their life time. Due to the limitation of our charging system, we were not able to charge the secondary circuit in 100 ms, therefore only the initial discharge had a prolonged lifetime. The succession of this long duration discharge followed by a consecutive laser-initiated discharge of shorter duration showed the following phenomenon: while the initial discharge is perfectly guided by the filament and a spark is observed, the second discharge follows a more erratic path and fails to reach the ground electrode, where no current is measured. This observation was confirmed by Schlieren imaging, as presented in Fig. 8 (a-b). An important background noise resulting from the heating of the initial discharge was observed during the second discharge propagation. Moreover, it is interesting to note that while the second discharge path was erratic, it stayed confined within the 2 cm wide hot channel formed by the first discharge heating. This measurement was repeated 5 times for all three values of C (720 nF, 540 nF, and 350 nF), but the second discharge was never observed to be guided and never reached the second electrode.

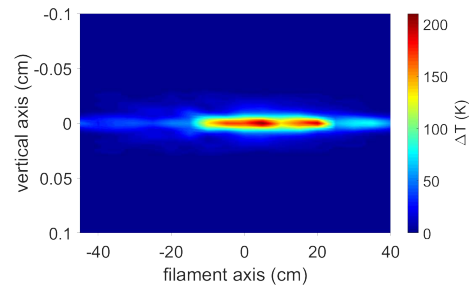


FIG. 9. Measurement of the temperature variation of the under-dense channel responsible for the guiding of the discharge, created by a 200 mJ, 780 fs, 800 nm laser pulse focused at 7 m. This measurement was done 1 s after the laser pulse.

To explain this phenomenon, it is important to recall that the density variation induced by laser filamentation^{22,23} is responsible for the guiding effect^{7,24,25}. By reducing the air density, the filaments define a path with a lower breakdown voltage²⁶ that will be followed by the discharge. To quantify this density variation in the condition of our experiment, we measured by transverse interferometry²⁵ the under-dense channel resulting from the filament heating over the 80 cm gap in the absence of a discharge. This system being at pressure equilibrium, we deduced from this measurement, presented in Fig. 9, an average temperature variation of 97 K and a maximum temperature variation of 210 K.

We then use the model of the discharge evolution described and tested previously to simulate the value of the discharge channel temperature 100 ms after the beginning of the discharge. The obtained values were 61 K for a short-lived discharge ($C = 0$) and 248 K for a long-lived discharge ($C = 720$ nF). It is then clear why we observed consecutive guided short-lived discharges and failed to see them when using long-

lived discharges: in the former case, the remaining heating of the initial discharge is less important than the heating due to the filament, thus the guiding effect is preserved. However, when using an initial prolonged discharge, the remaining heating is more important than the filament heating and the guiding effect is prevented. Similar conclusions can be done for prolonged discharges for capacitance value of 350 nF and 540 nF in the secondary circuit.

This adverse interaction could prevent the creation of a quasi-permanent conductive channel. However, being related to a thermal effect, it should be affected by an airflow sufficient to refresh the medium between consecutive discharges. We tested this hypothesis by using an air blower that creating a constant transverse airflow between the two electrodes with a speed varying from 3 m/s near the electrode to 6 m/s in the center of the gap. When the airflow was present, the negative interaction was successfully canceled and a guided discharge was generated following a long discharge, as presented in Fig. 8 (c). It is useful to note that even in this perturbed medium, the discharges were observed to be straight which could be of importance for outdoor application.

In conclusion, we have shown that injecting additional current into guided discharges can increase their lifetime to several milliseconds. We characterized the evolution of the discharge current, diameter and temperature by various measurements and developed a model to explain these evolutions. The generation of consecutive laser guided discharges separated by 100 ms was then studied. While successive short-lived discharges can be easily produced, the heating produced by a millisecond guided discharge prevents the guiding of the following one by the laser. We have shown that this adverse interaction can be suppressed by refreshing the air between consecutive laser shots.

ACKNOWLEDGMENTS

The authors acknowledge the European Union Horizon 2020 Research and innovation programme FET-OPEN under Grant No 737033-LLR and the French DGA under Grant No. 2018950901 EPAT3.

DATA AVAILABILITY

The data that support the findings of this study are available from the corresponding author upon reasonable request.

REFERENCES

- ¹A. Couairon and A. Mysyrowicz, "Femtosecond filamentation in transparent media," *Physics Reports*, **441**, 47–189 (2007).
- ²X. M. Zhao, J.-C. Diels, C. Y. Wang, and J. Elizondo, "Femtosecond ultraviolet laser pulse induced lightning discharges in gases," *IEEE J. Quantum Electron* **31**, 599 (1995).

- ³D. Comtois, C. Y. Chien, A. Desparois, F. Génin, G. Jarry, T. W. Johnston, J.-C. Kieffer, B. L. Fontaine, F. Martin, R. Mawassi, H. Pépin, F. A. M. Rizk, and F. Vidal, "Triggering and guiding leader discharges using a plasma channel created by an ultrashort laser pulse," *Applied Physics Letters* **76**, 819–821 (2000).
- ⁴T. Fujii, M. Miki, N. Goto, A. Zhidkov, T. Fukuchi, Y. Oishi, and K. Nemoto, "Leader effects on femtosecond-laser-filament-triggered discharges," *Phys. Plasmas* **15**, 013107 (2008).
- ⁵O. G. Kosareva, D. V. Mokrousova, N. A. Panov, I. A. Nikolaeva, D. E. Shipilo, E. V. Mitina, A. V. Koribut, G. E. Rizaev, A. Couairon, A. Houard, A. B. Savel'ev, L. V. Seleznev, A. A. Ionin, and S. L. Chin, "Remote triggering of air-gap discharge by a femtosecond laser filament and postfilament at distances up to 80 m," *Applied Physics Letters* **119**, 041103 (2021).
- ⁶A. Houard, P. Walch, T. Produit, V. Moreno, B. Mahieu, A. Sunjerga, C. Herkommer, A. Mostajabi, U. Andral, Y.-B. André, M. Lozano, L. Bizet, M. C. Schroeder, G. Schimmel, M. Moret, M. Stanley, W. A. Rison, O. Maurice, B. Esmiller, K. Michel, W. Haas, T. Metzger, M. Rubinstein, F. Rachidi, and J.-P. Wolf, "Laser-guided lightning," *Nat. Photonics*, 1–5 (2023).
- ⁷S. Tzortzakis, B. Prade, M. Franco, A. Mysyrowicz, S. Hüller, and P. Mor, "Femtosecond laser-guided electric discharge in air," *Phys. Rev. E* **64**, 57401 (2001).
- ⁸E. W. Rosenthal, I. Larkin, A. Goffin, T. Produit, M. C. Schroeder, J.-P. Wolf, and H. M. Milchberg, "Dynamics of the femtosecond laser-triggered spark gap," *Opt. Express* **28**, 54599–24613 (2020).
- ⁹T.-J. Wang, J. Zhang, Z. Zhu, Y. Liu, N. Chen, H. Guo, H. Sun, Y. Leng, S. L. Chin, and R. Li, "Femtosecond laser filament guided negative coronas," *AIP Advances* **10**, 035128 (2020).
- ¹⁰A. Schmitt-Sody, J. Elle, A. Lucero, M. Dmonkos, A. Ting, and et V. Hasson, "Dependence of single-shot pulse durations on near-infrared filamentation-guided breakdown in air," *AIP Adv.* **7**, 035018 (2017).
- ¹¹L. Arantchouk, G. Point, Y. Brelet, J. Larour, J. Carbonnel, Y.-B. André, A. Mysyrowicz, and A. Houard, "Compact 180-kV Marx generator triggered in atmospheric air by femtosecond laser filaments," *Appl. Phys. Lett.* **10**, 103506 (2014).
- ¹²Y. Brelet, A. Houard, G. Point, B. Prade, L. Arantchouk, J. Carbonnel, Y.-B. André, M. Pellet, and A. Mysyrowicz, "Radiofrequency plasma antenna generated by femtosecond laser filaments in air," *Appl. Phys. Lett.* **101** (2012).
- ¹³F. Théberge, J.-F. Gravel, J.-C. Kieffer, F. Vidal, and M. Châteauneuf, "Broadband and long lifetime plasma-antenna in air initiated by laser-guided discharge," *Appl. Phys. Lett.* **111** (2017).
- ¹⁴L. Arantchouk, B. Honnorat, E. Thouin, G. Point, A. Mysyrowicz, and A. Houard, "Prolongation of the lifetime of guided discharges triggered in atmospheric air by femtosecond laser filaments up to 130 μ s," *Appl. Phys. Lett.* **108**, 173501 (2016).
- ¹⁵L. Arantchouk, G. Point, Y. Brelet, B. Prade, J. Carbonnel, Y.-B. André, A. Mysyrowicz, and A. Houard, "Large scale tesla coil guided discharges initiated by femtosecond laser filamentation in air," *J. Appl. Phys.* **116**, 013303 (2014).
- ¹⁶F. Théberge, J.-F. Daigle, J.-C. Kieffer, F. Vidal, and M. Châteauneuf, "Laser-guided energetic discharges over large air gaps by electric-field enhanced plasma filaments," *Scientific reports* **7**, 1–8 (2017).
- ¹⁷Y. Brelet, A. Houard, L. Arantchouk, B. Forestier, Y. Liu, B. Prade, J. Carbonnel, Y.-B. André, and A. Mysyrowicz, "Tesla coil discharges guided by femtosecond laser filaments in air," *Appl. Phys. Lett.* **100** (2012).
- ¹⁸P. Castera and P.-Q. Elias, "Resistance models applied to the return stroke phase of negative pulsed surface discharges in air," *IEEE Trans. Plasma Sci.* **42** (2014).
- ¹⁹G. S. Romanov, Y. A. Stankevich, L. K. Stanchits, and K. L. Stepanov, "Thermodynamic and optical properties of gases in a wide range of parameters," *Int. J. Heat Mass Transf.* **38**, 545–556 (1995).
- ²⁰I. Sokolova, "Coefficients of air transfer in the range of temperatures from 3000 to 25 000 K and pressures 0.1, 1, 10, and 100 atm," *J. Appl. Mech. Tech. Phys.* **38**, 80–90 (1973).
- ²¹"Specair," <http://www.specair-radiation.net/>, accessed: 2023-01-27.
- ²²G. Point, C. Milián, A. Couairon, A. Mysyrowicz, and A. Houard, "Generation of long-lived underdense channels using femtosecond filamentation in air," *Journal of Physics B* **48**, 094009 (2015).

This is the author's peer reviewed, accepted manuscript. However, the online version of record will be different from this version once it has been copyedited and typeset.

PLEASE CITE THIS ARTICLE AS DOI: 10.1063/5.0146392

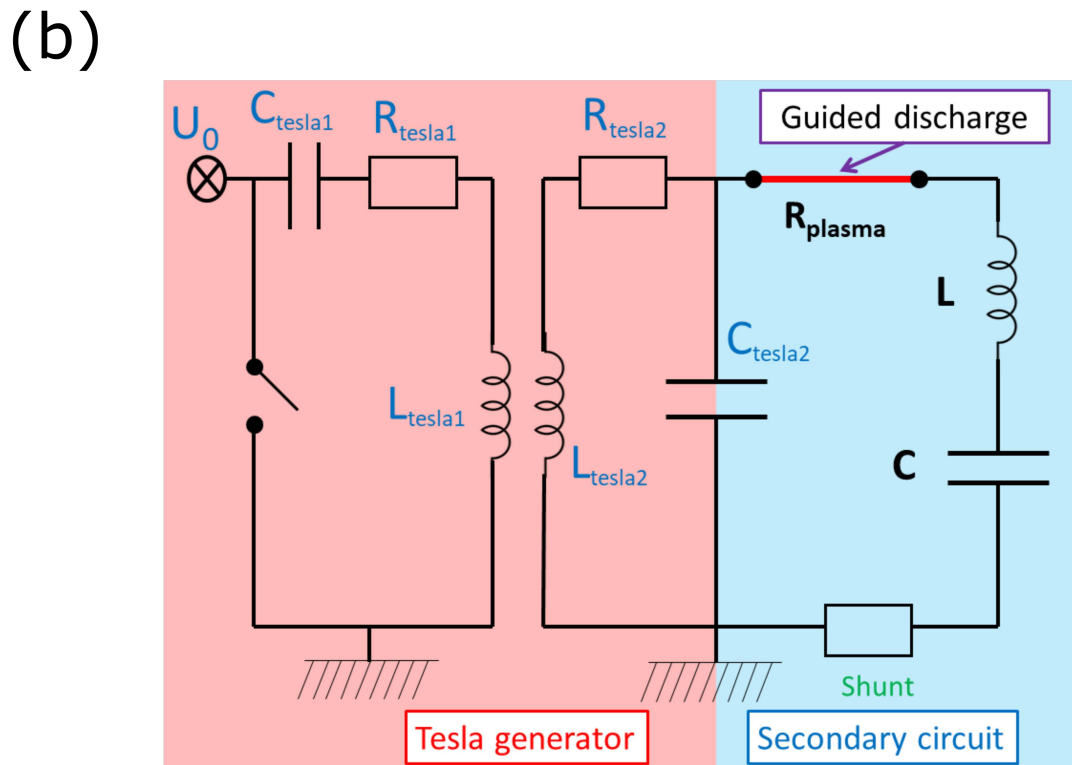
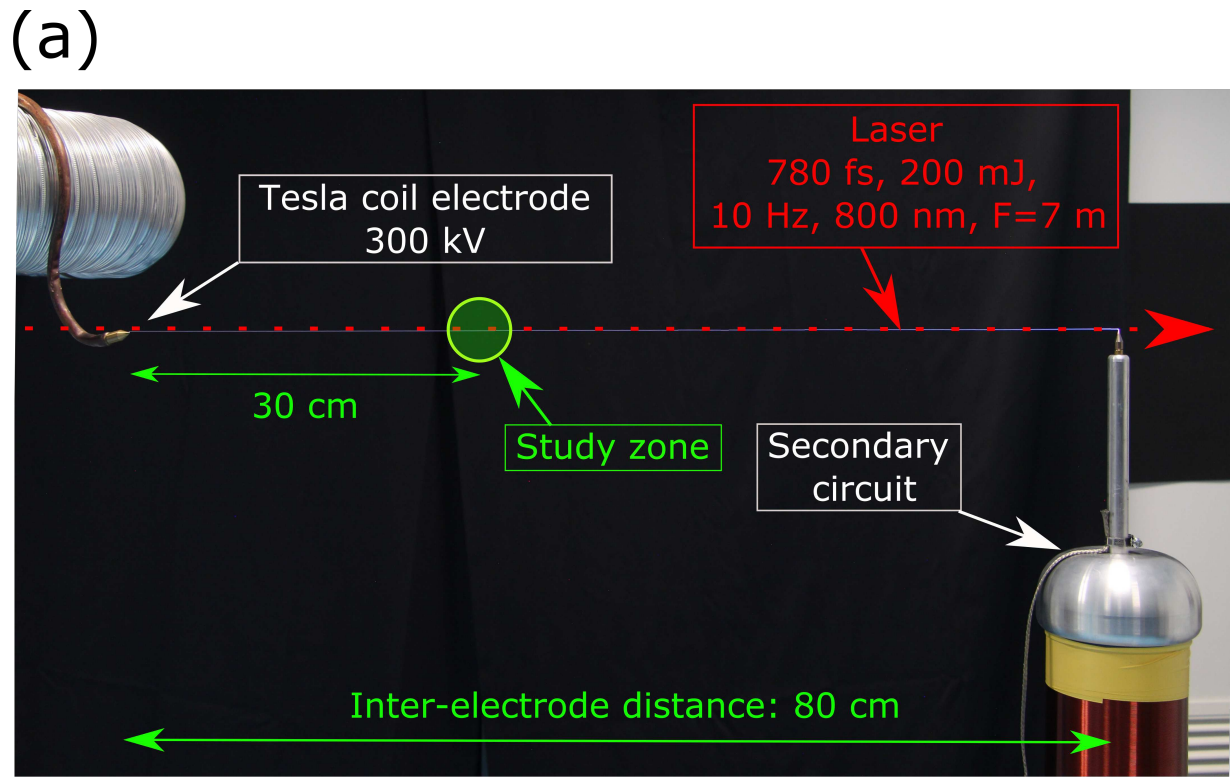
- ²³Y.-H. Cheng, J. K. Wahlstrand, N. Jhaji, and H. M. Milchberg, "The effect of long timescale gas dynamics on femtosecond filamentation," *Opt. Express* **21** (2013).
- ²⁴F. Vidal, D. Comtois, C.-Y. Chien, A. Desparois, B. L. Fontaine, T. W. Johnston, J.-C. Kieffer, H. P. Mercure, H. Pépin, and F. A. Rizk, "Modeling the triggering of streamers in air by ultrashort laser pulses," *IEEE Trans.*

Plasma Sci. **28**, 418 (2000).

- ²⁵P. Walch, B. Mahieu, L. Arantchouk, Y.-B. André, A. Mysyrowicz, and A. Houard, "Cumulative air density depletion during high repetition rate filamentation of femtosecond laser pulses: Application to electric discharge triggering," *Appl. Phys. Lett.* **119** (2021).

²⁶Y. P. Raizer, *Gas Discharge Physics* (Springer, 1991).

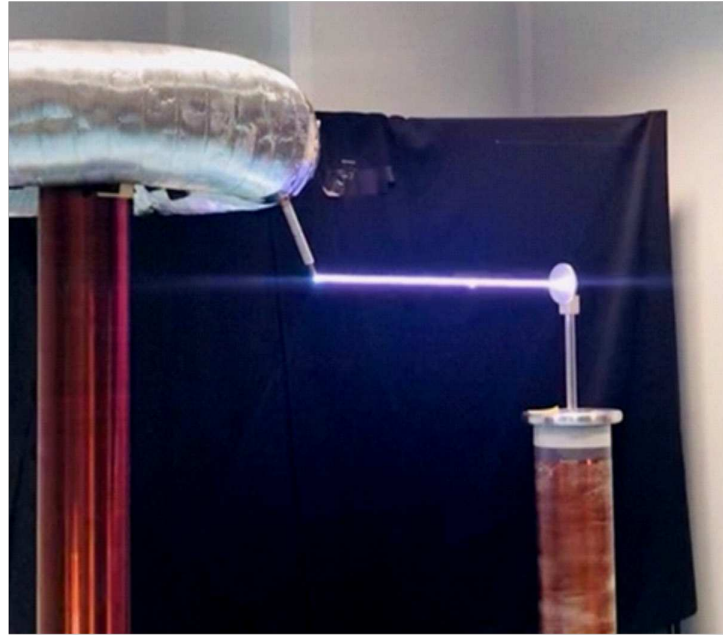
This is the author's peer reviewed, accepted manuscript. However, the online version of record will be different from this version once it has been copyedited and typeset.
 PLEASE CITE THIS ARTICLE AS DOI: 10.1063/5.0146392



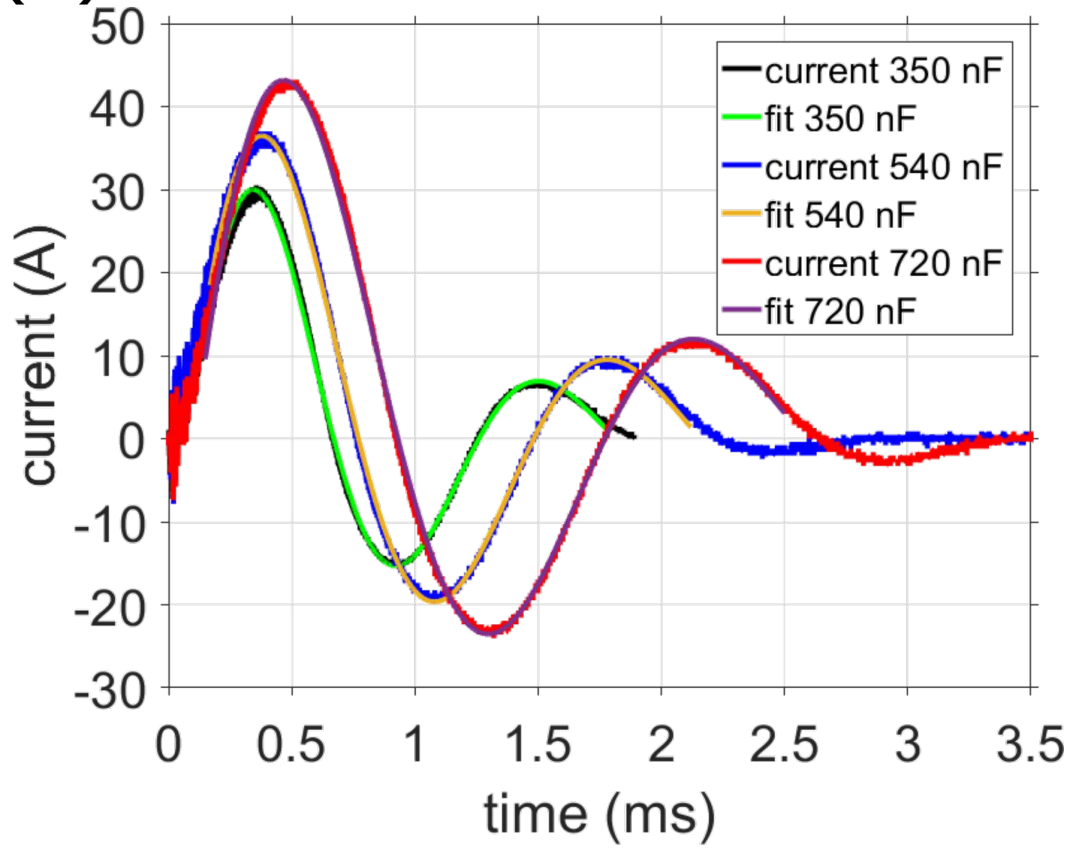
This is the author's peer reviewed, accepted manuscript. However, the online version of record will be different from this version once it has been copyedited and typeset.

PLEASE CITE THIS ARTICLE AS DOI: 10.1063/1.50146392

(a)

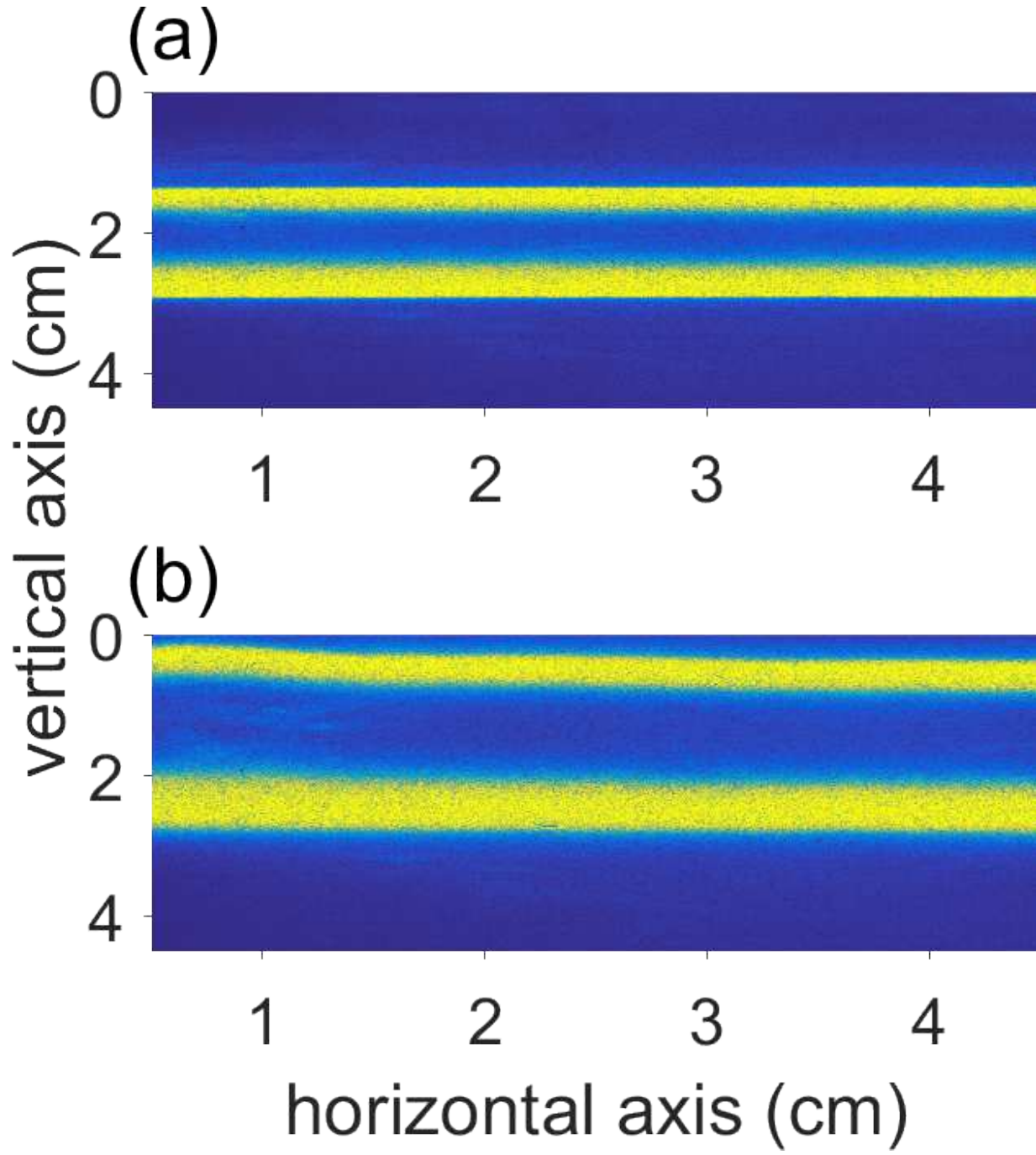


(b)



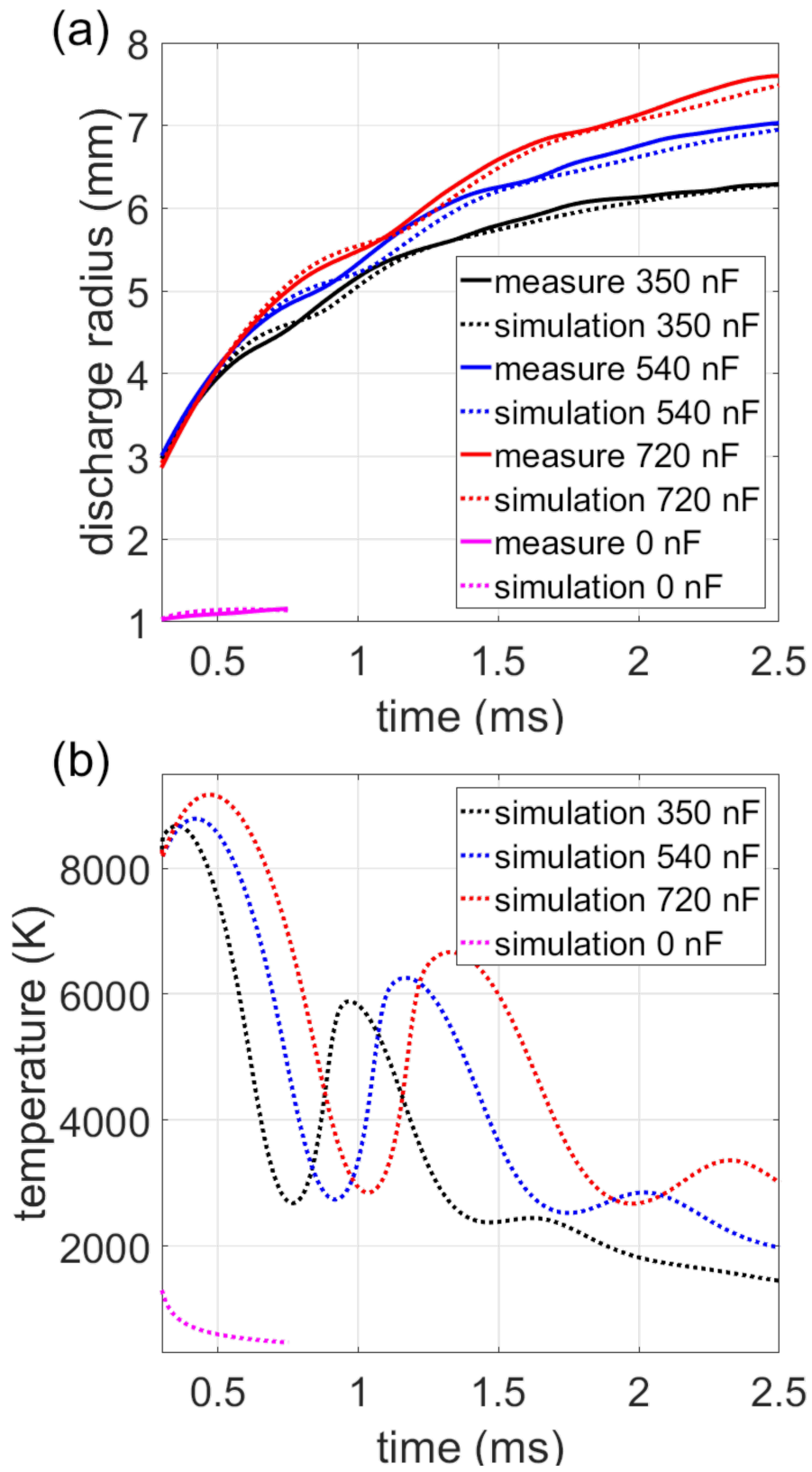
This is the author's peer reviewed, accepted manuscript. However, the online version of record will be different from this version once it has been copyedited and typeset.

PLEASE CITE THIS ARTICLE AS DOI: 10.1063/5.0146392

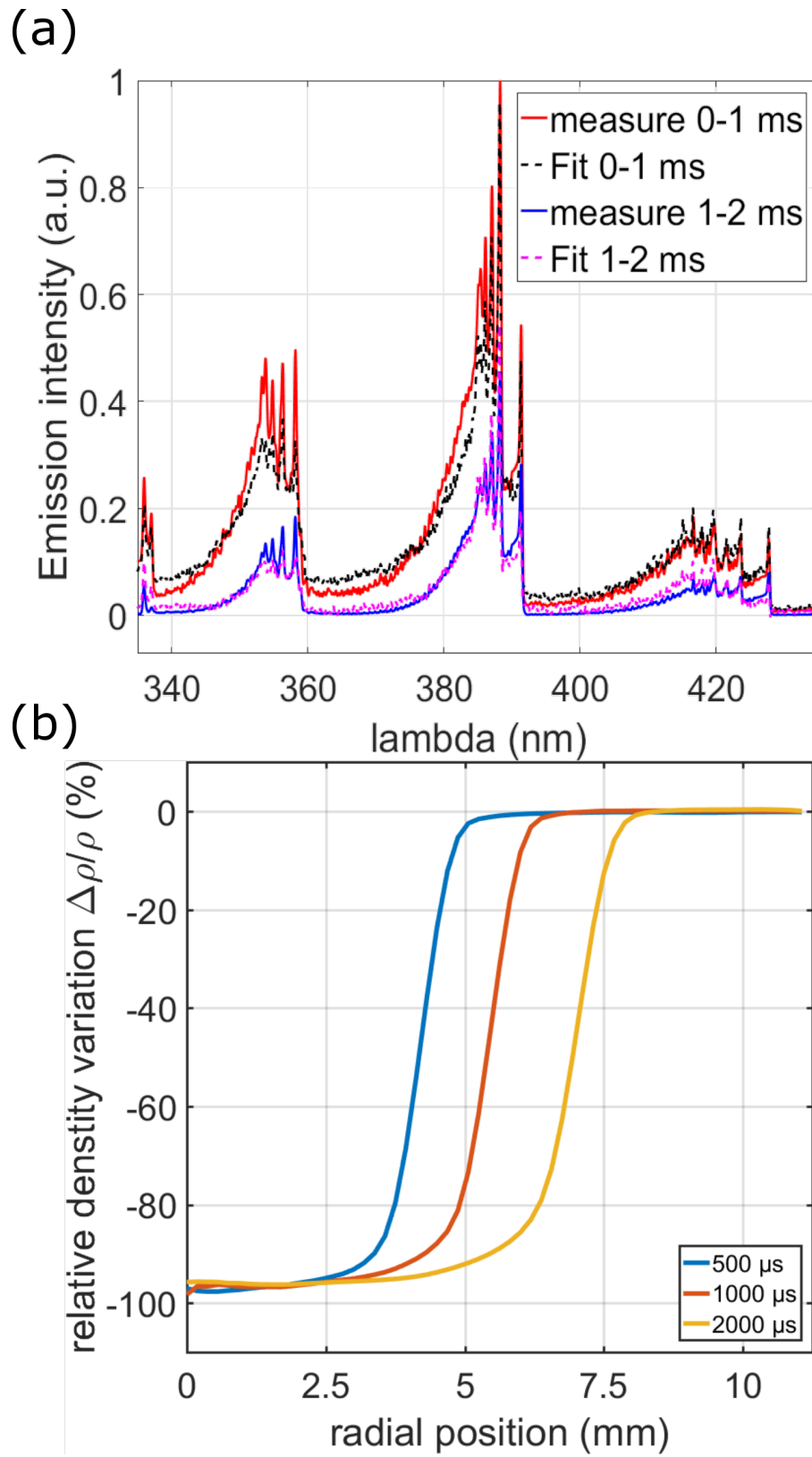


This is the author's peer reviewed, accepted manuscript. However, the online version of record will be different from this version once it has been copyedited and typeset.

PLEASE CITE THIS ARTICLE AS DOI: 10.1063/5.0146392

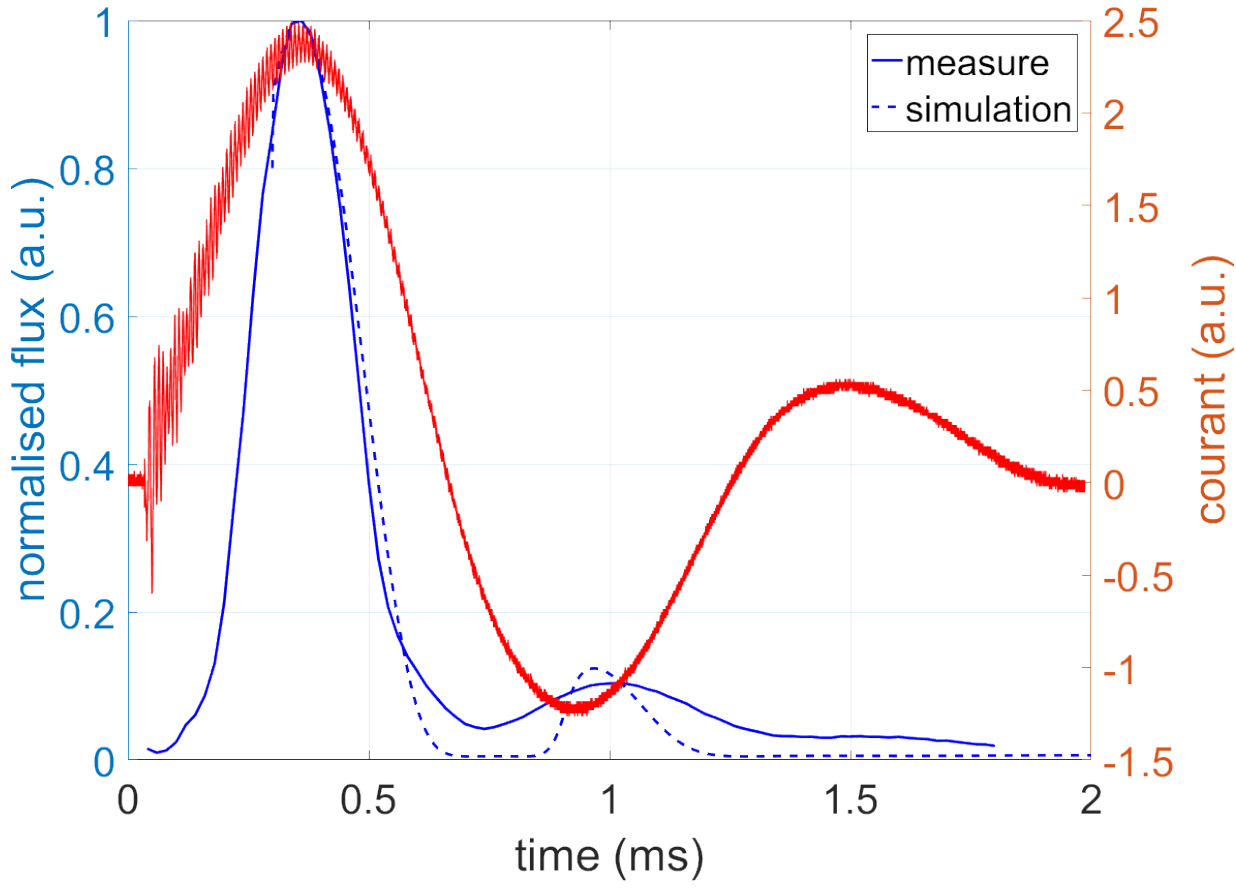


This is the author's peer reviewed, accepted manuscript. However, the online version of record will be different from this version once it has been copyedited and typeset.
 PLEASE CITE THIS ARTICLE AS DOI: 10.1063/5.0146392



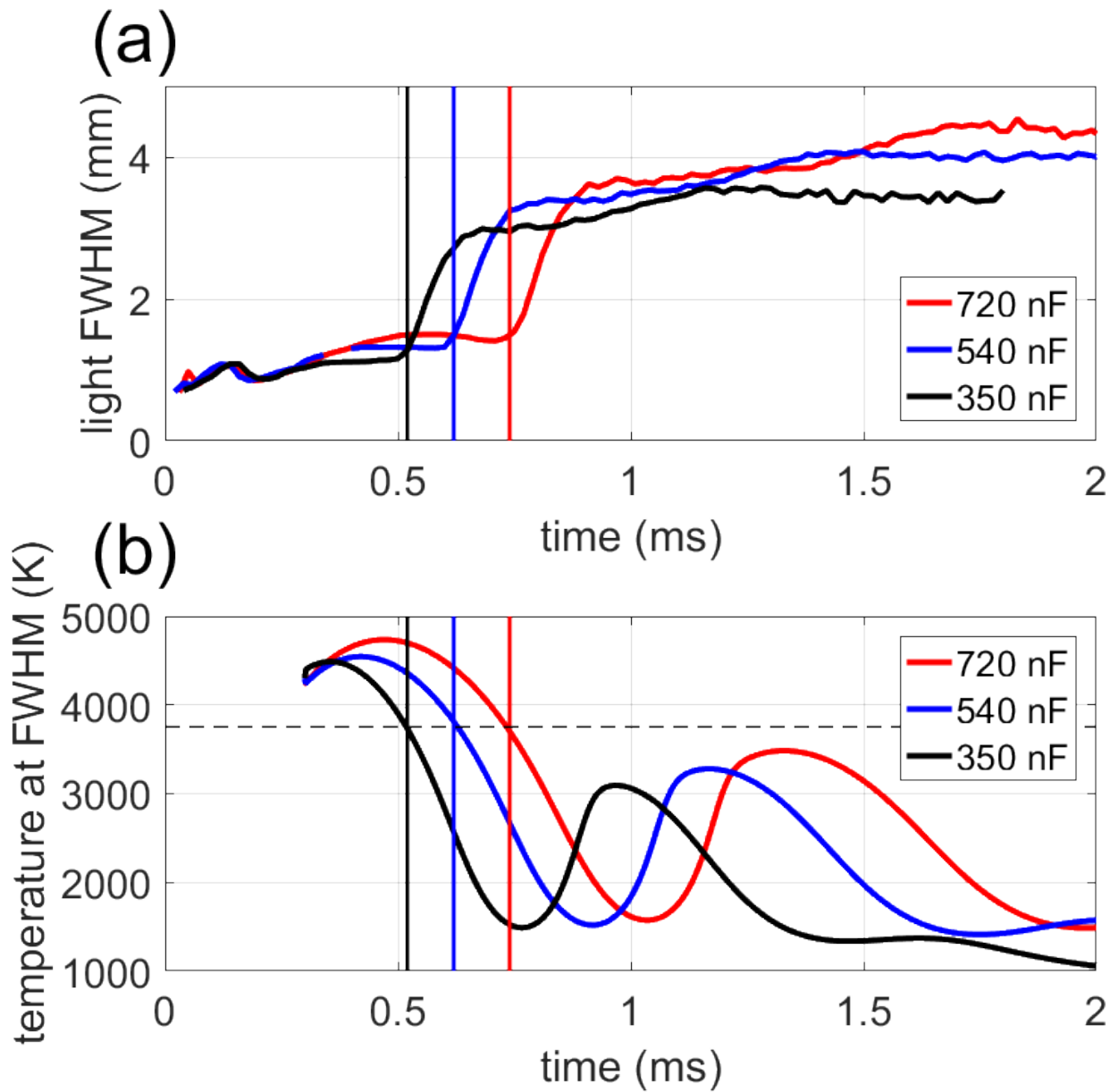
This is the author's peer reviewed, accepted manuscript. However, the online version of record will be different from this version once it has been copyedited and typeset.

PLEASE CITE THIS ARTICLE AS DOI: 10.1063/5.0146392



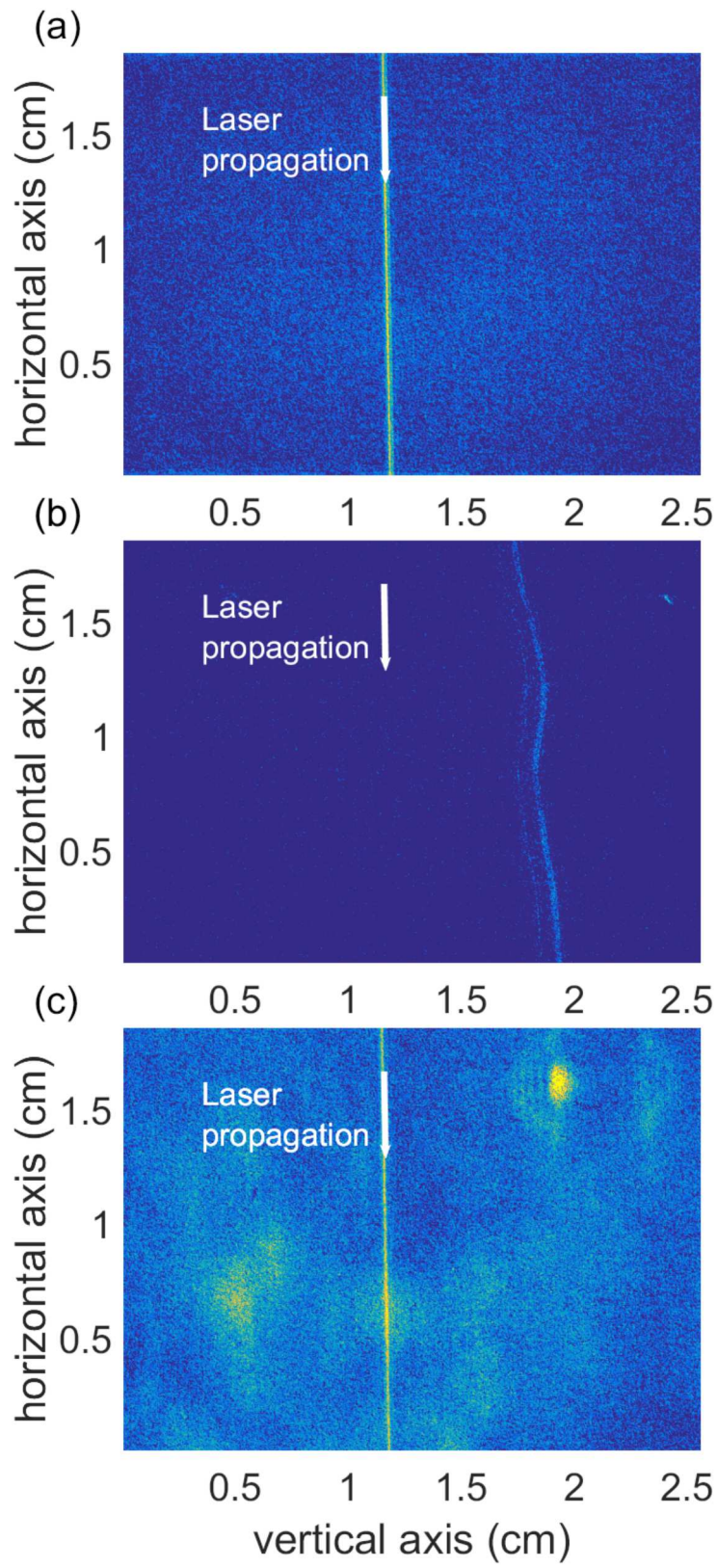
This is the author's peer reviewed, accepted manuscript. However, the online version of record will be different from this version once it has been copyedited and typeset.

PLEASE CITE THIS ARTICLE AS DOI: 10.1063/5.0146392



This is the author's peer reviewed, accepted manuscript. However, the online version of record will be different from this version once it has been copyedited and typeset.

PLEASE CITE THIS ARTICLE AS DOI: 10.1063/5.0146392



This is the author's peer reviewed, accepted manuscript. However, the online version of record will be different from this version once it has been copyedited and typeset.

PLEASE CITE THIS ARTICLE AS DOI: 10.1063/5.0146392

